Mon. Not. R. Astron. Soc. **286,** 384–392 (1997)

Analysis of galaxy formation with hydrodynamics

Patricia B. Tissera,[1,2]★ Diego G. Lambas[2] and Mario G. Abadi[2]

[1]*Department of Astrophysics, Nuclear & Astrophysics Laboratory, University of Oxford, Keble Road, Oxford OX1 3RH*
[2]*Consejo Nacional de Investigaciones Científica y Técnicas (CONICET) Observatorio Astronómico de la Universidad Nacional de Córdoba, Laprida 853, 5000 Córdoba, Argentina*

Accepted 1996 November 8. Received 1996 October 28; in original form 1996 March 5

ABSTRACT
We present a hydrodynamical code based on the smoothed particle hydrodynamics (SPH) technique implemented in an AP3M code that is aimed at solving the hydrodynamical and gravitational equations in a cosmological frame. We analyse the ability of the code to reproduce standard tests and perform numerical simulations to study the formation of galaxies in a typical region of a cold dark matter (CDM) model. These numerical simulations include gas and dark matter particles and take into account physical processes such as shock waves, radiative cooling and a simplified model of star formation. We analyse the astrophysical properties of the galactic objects in different models.

Key words: hydrodynamics – shock waves – methods: numerical – stars: formation – galaxies: formation – dark matter.

1 INTRODUCTION

The understanding of the physical processes involved in the formation and evolution of the structure in the Universe has signficantly improved over the last few years. The observational data available at present provide important information about the properties of the structure at different redshifts, encouraging the performance of more elaborate semi-analytical and numerical models. In particular, N-body simulations of hierarchical clustering models have allowed studies of a great variety of dynamical phenomena associated with galaxies and larger structures. In these simulations, a more consistent handling of both highly non-linear processes and a large dynamic range has been possible through the development of adequate numerical techniques and fast computers.

Numerical simulations of collisionless particles give a reliable description of the gravitational evolution of the dark matter component and have been significantly useful for the study of formation of structure in different cosmological models (Davis et al. 1985; Frenk et al. 1988; White & Frenk 1991; Tissera, Abadi & Lambas 1994). Although in these simulations the behaviour of the dissipative component is derived through simple modelling based on phenomenology, they have provided important clues for understanding the physical processes involved in the evolution of structure. In order to overcome some of the shortcomings of these models, hydrodynamics has been incorporated to purely gravitational codes by several authors (as examples see Evrard 1988, Hernquist & Katz 1989, hereafter HK, Cen et al. 1990, Summers 1994, Navarro & White 1993, Couchman, Thomas & Pearce 1995). Astrophysical problems require the use of numerical techniques to account for hydrodynamic effects because analytical approaches are restricted to systems with special symmetries. These techniques are a powerful tool for the study of fully non-linear hierarchical clustering when a gaseous component is present.

Smoothed particle hydrodynamics (SPH) is a widely used numerical method for the treatment of gas dynamics. It was first introduced by Gingold & Monaghan (1977) and by Lucy (1977) for the study of stellar pulsation, and only in the last decade has the SPH technique been applied to cosmological studies. Several implementations of SPH in tree, PP, PM, P3M and AP3M algorithms (e.g. Evrard 1988, HK, Umemura 1993, Navarro & Benz 1991, Thomas & Couchman 1992) can be found in the scientific literature. These implementations have provided the first insights in a more consistent treatment of systems with gas and dark matter.

Dissipative effects play a critical role in the evolution of the structure in galactic scales. They strongly affect the dynamical behaviour of the baryonic component making

★Current addresses: Universidad Autónoma de Madrid, Departamento de Física Teórica C-XI, Cantoblanco, Madrid 28040, Spain; Astrophysics Department, The Blackett Laboratory, Imperial College of Science, Technology and Medicine, Prince Consort Road, London SW7 2BZ.

possible the formation of rotationally supported discs (Katz 1992; Navarro & White 1994; Steinmetz & Muller 1995). Therefore, a complete picture of galaxy formation requires a full understanding of the accretion process of baryons into the potential wells of haloes. On the other hand, the hydrodynamical treatment of the dissipative component provides a more consistent framework to implement models for star formation. The transformation of cold gas into stars in dense regions is a critical process that influences many aspects of the evolution of galaxies, although a fully consistent treatment of these processes has not yet been achieved. A reliable model for star formation in numerical simulations is difficult to construct due to our poor understanding of the physics involved and the limits imposed by numerical resolution. Nevertheless, there have been several attempts at modelling star formation processes in SPH numerical simulations (Katz 1992; Navarro & White 1993; Steinmetz & Muller 1995). These authors have introduced schematic algorithms for transforming the cold gas in highly dense clumps into stars. Albeit simple, these algorithms provide a basic framework for the assessment of the effects of star formation processes on the properties of the galaxies, from which we can underpin a more realistic model.

In this paper we develop an implementation of SPH technique which follows in general terms the outline described by HK in the adaptative particle[3] mesh code (AP3M) developed by Couchman (1991). In Section 2, we present a brief description of SPH and of the implementation performed in this paper. Section 3 describes the tests of the code. In Section 4 we study the formation of galaxies in a typical region of the Universe without considering star formation. In Section 5 we introduce a simple star formation scheme and analyse general astrophysical properties of the resulting galactic-size objects. Section 6 outlines the main conclusions.

2 SPH IMPLEMENTATION

SPH is a purely Lagrangian method which allows straightforward numerical integration of the hydrodynamics equations of a continuous fluid. Several authors have discussed in detail the derivation of the SPH equations from the hydrodynamics ones (see, for instance, Benz 1990). In this section, we restrict ourselves to outlining the main characteristics of our implementation, assuming that the reader is familiar with previous works (Evrard 1988; HK; Navarro & Benz 1991; Couchman et al. 1995). Nevertheless, a detailed description can be found in Tissera (1995). We have followed in general terms the implementation presented by HK, although relevant aspects discussed by other authors has been taken into account.

The smoothed value of the physical variables of an element of fluid represented by a particle can be estimated basically upon the knowledge of the kernel, its derivatives and the physical information provided by the neighbouring particles. Hence, the key point in SPH is to provide an algorithm to effectively construct the list of particle neighbours.

A smoothing length varying both in space and time, $h(r, t)$, has been assigned to each particle. The evolution of $h(r, t)$ depends on the history of the particle and has been estimated similarly to Navarro & White (1993). We also control that the lists of neighbours defined by $h(r, t)$ always contain 30–50 gas particles for every particle at any time of the simulations.

A B-spline kernel (Monaghan & Latanzio 1985) has been used due to its mathematical advantages over other possibilities, such as Gaussian ones (mainly because of its compact support definition). Similar to HK we symmetrize the kernel contributions in order to try to avoid violations of energy conservation due to numerical artefacts.

An artificial viscosity has been introduced in order to accomplish a numerically correct description of the evolution of the fluid in a discontinuity layer (Monaghan & Gingold 1983). The inclusion of this artificial viscosity force makes possible the numerical resolution of shocks, generating the correct exchange of energies and damping non-physical oscillations on the scale of the particle separation. We have adopted the following functional form proposed by Monaghan & Gingold:

$$\Pi_{ab} = \begin{cases} \dfrac{-\alpha c_{ab}\,\mu_{ab} + \beta\mu_{ab}^2}{\rho_{ab}} & \boldsymbol{v}\cdot\boldsymbol{r} \leq 0 \\ 0 & \text{otherwise,} \end{cases}$$

where

$$\mu_{ab} = \frac{h\boldsymbol{v}_{ab}\cdot\boldsymbol{r}_{ab}}{r_{ab}^2 + \eta h^2}. \tag{1}$$

where $\boldsymbol{r}$ and $\boldsymbol{v}$ are the position and velocities of particles; $\alpha=1$, $\beta=1$ and $\eta=0.01$ are dimensionless constants; and $c_{ab}=0.5\ (c_a+c_b)$ and $\rho_{ab}=0.5\ (\rho_a+\rho_b)$ are the mean pair sound speed and the pair-averaged density, respectively.

In order to compute the effects of the radiative cooling, we adopt the approximation for the cooling function, $\Lambda(\epsilon)$, given by Dalgarno & McCray (1972), for a primordial mixture of hydrogen and helium [He/(H + He) = 0.25]. In the case where dissipative processes are present, the integration of (1) demands extra caution. Taking into account this fact, we have updated the internal energy ϵ using a semi-implicit integration method based on a predictor–corrector scheme (HK). Since the AP3M code uses the same time-step for all particles, this semi-implicit method allows us to follow more carefully the integration of the internal energy. This is particularly important for particles situated in high-density regions where cooling time-scales are shorter than dynamical time-scales.

We have implemented the contribution of hydrodynamical forces into the AP3M code using a standard leapfrog algorithm to update particle positions and velocities. The cosmic energy equation for a fluid in comoving coordinates (Peebles 1980) modified to take into account the gas pressure and radiative energy losses is used for checking the performance of the integration throughout the simulations.

3 SELF-SIMILARITY SOLUTIONS FOR AN ADIABATIC SPHERICAL COLLAPSE

The reproduction of the self-similarity solutions of an adiabatic spherical collapse has become a classic test for hydrodynamical codes in three dimensions. Bertschinger (1985) studied the evolution of a spherical perturbation in an otherwise uniform Einstein–de Sitter universe model, finding the following self-similarity solutions for the evolution of the pressure (p), density (ρ), mass (m) and velocities (v) fields in the secondary accretion collapse:

$$v(r,t)=\frac{r_{\mathrm{ta}}}{t}V(\lambda) \tag{2}$$

$$\rho(r,t)=\rho_{\mathrm{H}}D(\lambda) \tag{3}$$

$$p(r,t)=\rho_{\mathrm{H}}\left(\frac{r_{\mathrm{ta}}}{t}\right)^2P(\lambda) \tag{4}$$

$$m(r,t)=\frac{4}{3}\pi\rho_{\mathrm{H}}r_{\mathrm{ta}}^3M(\lambda), \tag{5}$$

where

$$\rho_{\mathrm{H}}=(6\pi Gt^2)^{-1} \tag{6}$$

$$r_{\mathrm{ta}}(t)=\left(\frac{3\pi}{4}\right)^{-8/9}\delta_{\mathrm{i}}^{1/3}r_{\mathrm{i}}\tau^{8/9} \tag{7}$$

$$\lambda=\frac{r(t)}{r_{\mathrm{ta}}(t)}, \tag{8}$$

where the subscripts 'i' and 'ta' denote initial and turn-around times, respectively.

We have simulated the collapse of a spherical adiabatic perturbation of a collisional fluid in order to compare the results of our code with these semi-analytic solutions. We have followed the accretion of an initially uniform distribution of $N=4096$ gas particles on to a central perturbation with a density contrast $\delta\rho/\rho\simeq5$, and computed the parametrized functions $V(\lambda)$, $D(\lambda)$, $P(\lambda)$ and $M(\lambda)$ at different stages of the evolution.

Fig. 1 shows the analytical solutions found by Berstschinger (solid lines) and the relations obtained from the simulations at different times that correspond to $N_{\mathrm{gas}}\simeq200$, 300 and 400 particles inside the shock radius ($r_{\mathrm{s}}=0.34r_{\mathrm{ta}}$). As we can see in this figure, the fit to the theoretical solutions improves as the number of particles inside the radius shock increases. A disagreement between numerical and analytical results in the distributions of $V(\lambda)$, $D(\lambda)$ and $P(\lambda)$ can be observed in the shock discontinuity region, mainly due to numerical resolution problems (see also fig. 1 in Navarro & White 1993 and fig. 7 in Couchman et al. 1995). In spite of this fact, particles enter and reach a state of equilibrium with the correct smoothed values for the physical variables predicted by the theory. This fact reassures us that the code is reproducing satisfactorily the jump in the physical properties of the fluid at a discontinuity layer.

4 CDM NUMERICAL SIMULATIONS

In this section, we study the formation of galactic objects in a typical region of a cold dark matter (CDM) model follow-

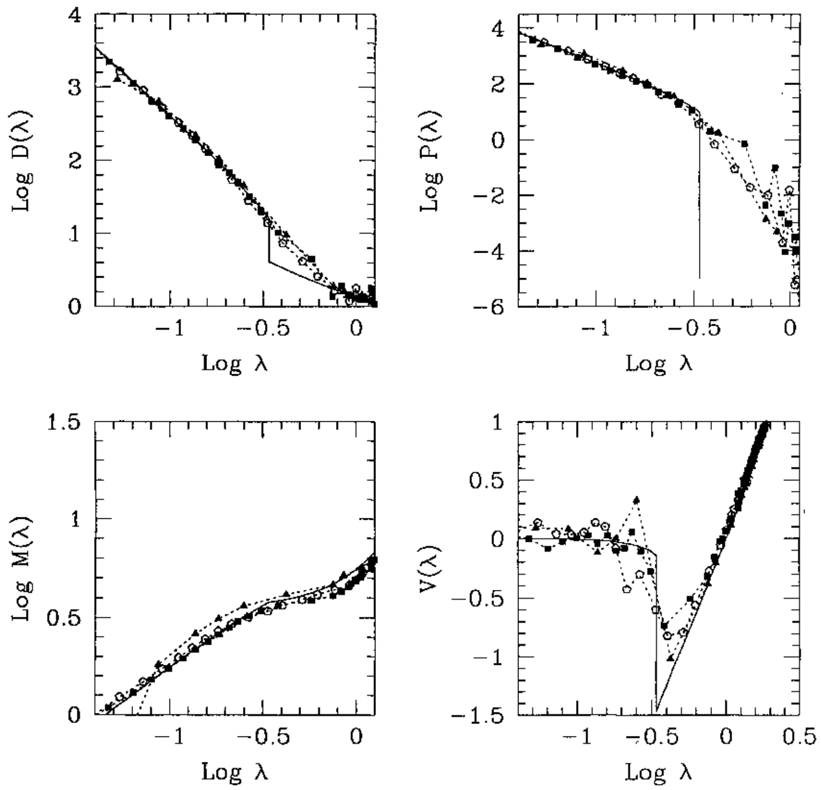

Figure 1. Self-similarity solutions for an adiabatic spherical collapse for density (D), pressure (P), mass (M) and velocity (V) fields. Simulated solutions for different particle numbers inside the r_{s} are shown: $N\simeq200$ (filled triangles), $N\simeq300$ (open pentagon) and $N\simeq400$ (filled squares). Analytical solutions are shown for comparison (solid line).

ing the evolution of dark and baryonic matter. We analyse two different models. Model A deals with the gravitational and hydrodynamic evolution of the matter including the treatment of pressure gradients, shocks and radiative cooling, whereas Model B also introduces a schematic algorithm to take into account the effects of star formation processes.

The initial conditions of the simulations correspond to a biased CDM power spectrum with a density parameter $\Omega=1$ and a zero cosmological constant $\Lambda=0$ (we adopt a Hubble's constant $H=50$ km s^{-1} Mpc^{-1}). We set initial positions and velocities for $N=64^3$ particles according to the Zel'dovich approximation in a computational box of $L=10$ Mpc and 64^3-particle grid with periodic boundary conditions. Dark and gas particles have equal masses, $m=2.6\times10^8$ M$_\odot$. Gas particles are selected at random from the initial conditions according to a baryon density parameter $\Omega_b=0.1$. The simulations were evolved until the rms mass fluctuations reached a value of 0.4 in a sphere of radius 16 Mpc (bias parameter $b=2.5$). The softening length for the gravitational forces is $\simeq 5$ kpc fixed in physical units. Table 1 summarizes the main characteristics of the simulations performed.

Table 1. Simulations.

Sim	Npart	Ω_b	b	c	ρ_{crit}
1	64^3	0.1	2.5	-	-
2	64^3	0.1	2.5	-	-
3	64^3	0.1	2.5	1	710^{-26}
4	64^3	0.1	2.5	0.03	710^{-26}
5	64^3	0.1	2.5	0.05	710^{-26}
6	64^3	0.1	2.5	0.01	710^{-26}

4.1 Model A without star formation

We first analyse simulations without including star formation processes. This model is a first approach to the study of the formation of structure on galactic scales. In Fig. 2 are shown the projected distributions of the dark matter (Fig. 2a) and the baryonic particles (Fig. 2b) at redshift ($z=0$) for a subregion of size $L\simeq 3$ Mpc of simulation 1. Due to the high efficiency of the radiative cooling, most of the gas in high-density regions remains at the minimum allowed temperature, $T\simeq 10^4$ K. In Fig. 2(b) it can be seen that the cold gas settles into clumps that are easily individualized. If we look more carefully at those small clumps, disc-like structures may be identified. Figs 2(c) and (d) show the projected distribution of particles corresponding to a zoomed region of 500 and 150 kpc box size, respectively. Although our dynamical resolution range is not as high as desired, the formation of disc systems can be followed quite well in massive objects ($M_{gas}>4\times10^{10}$ M$_\odot$).

We have identified galactic haloes applying an algorithm based on a density contrast criteria, $\delta\rho/\rho\propto 200$ (White & Frenk 1991; Lacey et al. 1993). Table 2 summarizes the principal characteristics of two clumps, haloes 1 and 2, which will be analysed in detail henceforth.

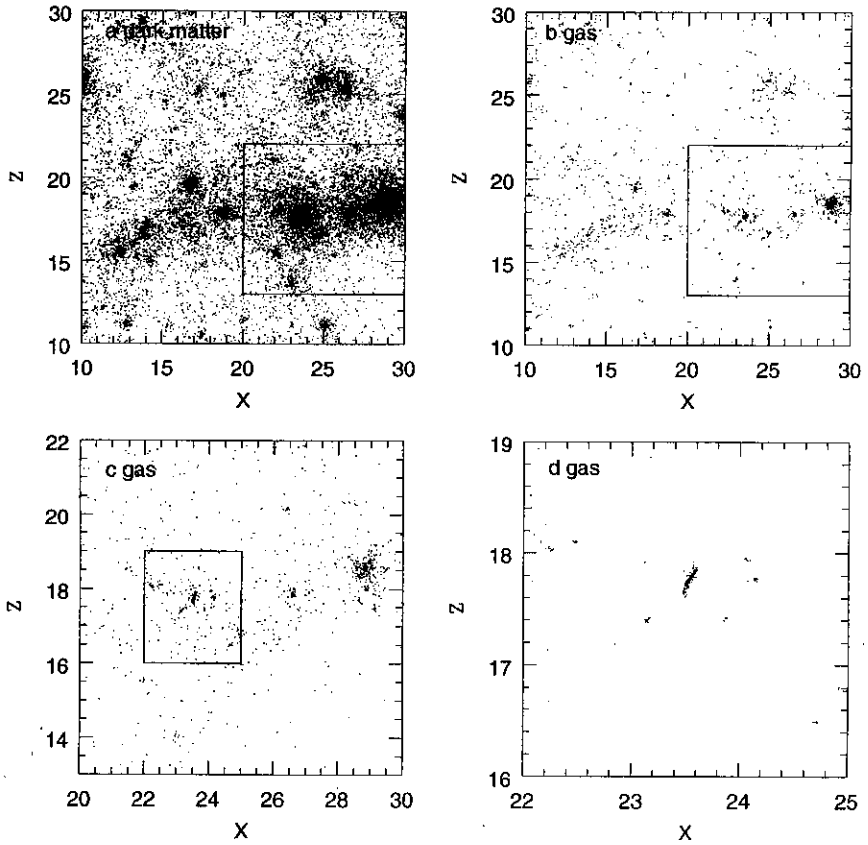

Figure 2. Projected distribution of (a) dark matter and (b) gas particles in a subsample of $L=3$ Mpc of simulation 1; (c) and (d) are closer views of the subregions delimited by the boxes.

Table 2. Parameters of haloes 1 and 2 at $z=0$ [M_T, M_b, M_{gas} and $V_c=(GM/R)^{1/2}$ have been measured at the virial radius; K_{tot} and K_{rot} have been calculated for the discs assuming a fixed radius of 30 kpc].

Sim	H	M_b $10^{12}M_o$	M_T $10^{12}M_o$	M_b/M_T	R_{Vir} (kpc)	λ	V_c (km/sec)	K_{rot}/K_{tot}
1	1	0.27	2.21	0.12	322	0.02	169	0.95
	2	0.23	1.9	0.12	300	0.06	161	0.98
Sim	**H**	**M_* $10^{12}M_o$**	**M_T $10^{12}M_o$**	**M_b/M_T**	**R_{Vir} (kpc)**	**λ**	**V_c (km/sec)**	**M_{gas}/M_{tot}**
3	1	0.22	2.19	0.12	317	0.02	168	0.027
	2	0.17	1.93	0.12	317	0.05	161	0.03
4	1	0.22	2.19	0.12	317	0.02	168	0.03
	2	0.15	1.79	0.12	309	0.04	158	0.04
6	1	0.07	2.21	0.12	322	0.02	169	0.06
	2	0.08	1.9	0.11	305	0.06	162	0.085

We traced back in time the evolution of the particles belonging to haloes identified at $z=0$ in order to study their formation history. Disc-like structures form as the result of the hierarchical aggregation of substructure and mergers with other objects. As an example, Figs 3(a), (b) and (c) show the evolution of gas particles belonging to halo 2. We can see in these figures two disc objects at $z=0.17$, the result of their merger at $z\simeq0.08$ and the final configuration at $z=0$.

This example shows that gaseous discs can be regenerated after mergers of two initial disc-like objects as pointed out by Navarro & White (1994). We also observe that when a merger occurs the compact cold gas clumps orbit around each other before the merger effectively happens. It can be seen that several galaxy-like objects in our simulations have satellite neighbours inside r_{200} that have been recently captured (r_{200} is the radius of the sphere in which the density contrast satisfied the condition $\delta\rho/\rho\propto200$).

We have calculated the ratio between the rotational kinetic energy (K_{rot}) and the total kinetic energy (K_{tot}) of the disc structures obtaining typical values greater than 0.5. In particular, haloes 1 and 2 have $K_{rot}/K_{tot}\simeq1$ as shown in Table 2, indicating that these disc systems are rotationally supported. On the other hand, we have estimated the ratio of baryonic mass to total mass inside the virialized region of haloes (M_b/M_{vir}) to be $\simeq0.11$–0.12, which is consistent with the mean baryonic density parameter $\Omega_b=0.1$, albeit slightly greater. We find that the cold gas mass is more concentrated than dark matter reaching comparable values at a radius $r\simeq10$–15 kpc.

According to White & Frenk (1991) the virial mass (M_{vir}) of a halo formed at redshift z can be expressed as a function of its circular velocity, $V_c(\mathrm{km\ s^{-1}})=(GM/R)^{1/2}$, measured at the virial radius:

$$M_{vir}[\mathrm{M}_\odot]=2.35(1+z)^{-3/2}V_c^3 10^5\,\mathrm{M}_\odot\ h^{-1}. \quad (9)$$

In our simulations, we find that the gas that has settled in haloes also satisfies this relation ($M_{gas}\propto V_c^3$). It should be remarked that the total cold gas mass in the simulated haloes exceeds by a factor of 5 the total observed stellar mass content of galaxies of comparable circular velocity. So, if it were assumed that the total accreted gas mass in the simulated haloes was gradually being transformed into stars, the resulting stellar content would be in open disagreement with observations. This problem may be overcome by introducing heating sources such as supernovae which may prevent the gas from overcooling and settle into the potential well of the haloes from early times.

4.2 Model B including star formation

Star formation is a critical factor in the evolution of the galactic structure. The physical processes involved are a key point in the study of galaxy formation, although they are still not well understood. Moreover, it is difficult to model them realistically taking into account the current computational resolution ranges. In this Section, we introduce a simple star formation (SF) algorithm but for reasons of simplicity we have not considered stellar feedback processes.

Our prescription of SF is based on the model described by Navarro & White (1993). Following these authors, a gas particle is assumed to be in the process of forming stars if the Jeans instability condition is satisfied and if its cooling time is shorter than its dynamical time. A critical density ($\rho_{crit}\simeq7\times10^{-26}$ g cm^{-3}) can be estimated such that if $\rho_{gas}\geq\rho_{crit}$, the second condition is satisfied. It is assumed that the Jeans instability condition is fullfilled if the gas particle is in a convergent flow ($\nabla\cdot\boldsymbol{v}<0$).

Once a particle representing a gas cloud satisfies these requirements, it is transformed into stars according to a certain star formation rate (SFR). We assume the following SFR:

$$\frac{\mathrm{d}\rho_{gas}}{\mathrm{d}t}=-c\frac{\rho_{gas}}{t_*}, \quad (10)$$

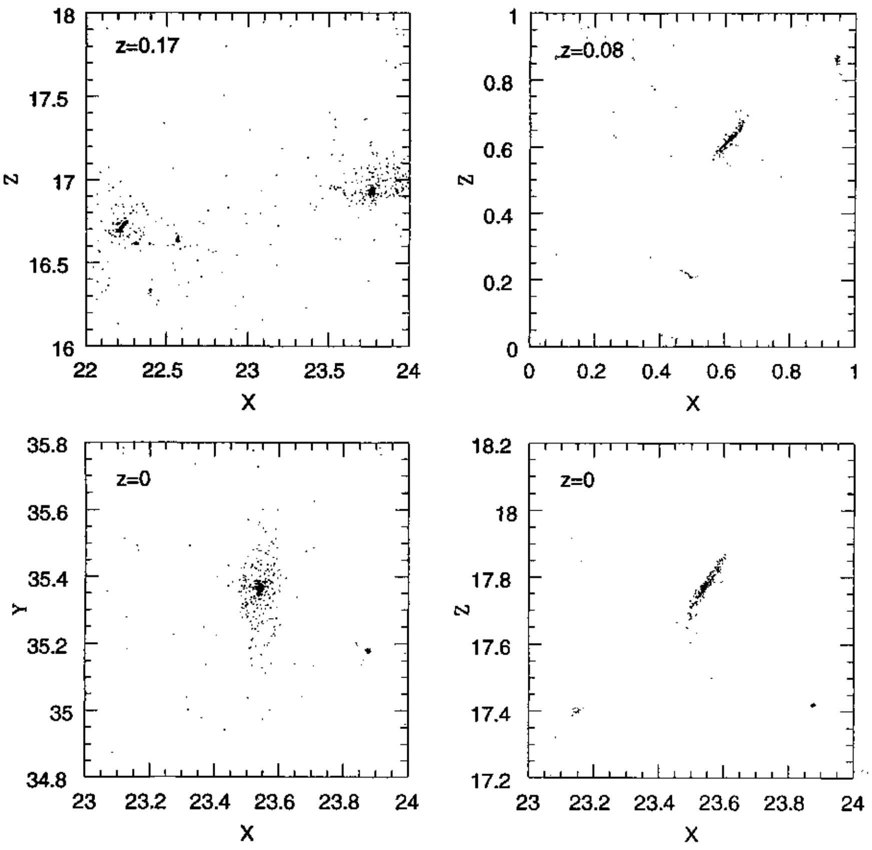

Figure 3. History of formation of halo 3. (a) Two colliding discs at $z=0.17$. (b) The result of the merger at $z=0.8$. (c) and (d) Final configuration of disc at $z=0$ (planes xy and xz, respectively).

where c is a dimensionless star formation rate parameter and t_* is a characteristic time-scale which is assumed to be equal to the dynamical time-scale of the gas cloud represented by the particle, $t_g \propto \rho_{gas}^{12}$. We assume that a gas particle is transformed instantaneously into stars after a time interval (τ) over which the gas mass is expected to be transformed into stars according to equation (10) (Navarro & White 1994).

4.2.1 *Analysis*

In order to analyse the effects of the star formation efficiency, we have performed several simulations that share the same initial conditions but have different values of the efficiency parameter c (Table 2). The SF scheme described above may be very efficient in transforming the gas into stars. This high efficiency could lead to spurious results if stars are formed at early stages of the evolution, producing an excess of stellar mass and inhibiting the formation of disc structures.

We identified galactic haloes at different redshifts using the algorithm previously mentioned. Table 2 summarizes the main characteristics of the haloes 1 and 2 at $z=0$.[1] The detailed analysis of the properties of galactic haloes is being carried on by Tissera & Dominguez (in preparation). As a consequence of our hydrodynamical resolution range, the evolution of the gas inside haloes with V_c of less than $\simeq 50$ km s^{-1} (or $M_{vir} \leq 10^{11}$ M$_\odot$) cannot be well represented. This fact may artifically delay the start of the process of star formation. The maximum star formation rate is reached on average at $z \simeq 1$. At this redshift approximately 8 per cent of the total baryonic mass has been transformed into stars. This fraction increases to 15–30 per cent at $z=0$, producing a baryonic density parameter estimated from stars in simulated galaxies of $\Omega_* \sim 0.015$–0.03, while the observed value is $\Omega_* \simeq 0.004$ (Peebles 1993). This significant excess of stars can be related to the overcooling effect discussed by several authors (Cole 1994; Navarro & White 1994) which generates an early collapse of the gas into the clumps. On average, the total cold gas mass in the simulated galaxies at $z=0$ is approximately 45–50 per cent of the total baryonic mass in the volume considered. Heating processes like supernova explosions or photoionization might prevent the gas from overcollapsing into small dense cold clumps reducing the amount of matter capable of forming stars.

The use of different efficiency parameters c generates different histories of star formation implying differences in the astrophysical properties of the final objects. A high SF efficiency can transform the gas into stars rapidly enough to produce spheroidal structures. An adequate adjustment of this parameter allows the gas to settle into a disc-like struc-

[1]The data displayed in Table 2 correspond to simulations sharing the same initial conditions but having different star formation efficiency parameters. Simulations 2 and 5 have not been included since their initial conditions are different.

ture while being transformed into stars. We have not imposed any physical constraint in order to choose a value of c but have analysed a range of possible ones with the aim of assessing its influence on the properties of the objects. Fig. 4(a) shows the distributions of dark matter, gas and star components of halo 3 in simulation 6 where a gaseous disc and a bulge of stars could be formed with a particular value of c. Fig. 4(b) shows the same object in simulation 3. The star formation efficiency parameters used in these two runs are quite extreme (Table 1) and, therefore, show clearly the physical differences of the objects depending on c (apart from the fact that the satellites in simulation 3 have been able to form stars). In model 1, stars are formed in the dense cores of the galactic objects while in model 2 the number of stars is higher and they are more extensively distributed. Complementarily, the fraction of gas left over is greater in model 1. These results show how sensitive the properties of galactic objects are to models and, hence, how artificial the conclusions derived from them may be. In particular, we think that the value of c needs to be set according to physical constraints (Mosconi, Tissera & Lambas 1994; Kauffmann, White & Guiderdoni 1993). In simulation 6 the maximum of the SF rate is reached at a low redshift ($z \simeq 0.3$). This artificial delay of the SF processes implies a more recent SF history that does not agree with observations but has been carried out as an extreme example. On the other hand, in these models massive discs settle at $z \geq 0.5$ on average, in agreement with the conclusions of Navarro & White (1993). This result may be affected by several factors including numerical resolution, so more detailed simulations are required to more consistently address this problem.

4.2.2 *Astrophysical properties*

We estimate the luminosities of simulated galaxies in different bands taking into account the stellar evolutionary tracks computed by Charlot & Bruzual (1991). These analytical tracks give the evolution of the luminosity per unit mass as a function of age for a given initial mass function (IMF) and mass-to-luminosity ratio. For each star particle, we compute the corresponding luminosities at each time-step taking into account its formation redshift. We derive the total luminosities of galactic objects adding the individual luminosities of each star particle inside r_{200}. We adopt a Miller–Scalo (Miller & Scalo 1979) initial mass function with a lower mass cut-off of 0.1 $M_{\odot}$ and an upper mass cut-off of 125 $M_{\odot}$. A single burst of star formation lasting 1.2×10^7 yr has been assumed to occur in each particle. We do not consider gas metallicity enrichment.

The Tully–Fisher (TF) relation for galaxies also provides a confrontation between models and observations. Several authors have found fits to this relation in different bands (see for instance Pierce & Tully 1992). It is observed that the slope and the zero-point of the fits to the TF relation may vary over an important range of possible values.

As a first step towards understanding the physics involved in the TF relation, we have analysed the dependence of the total baryonic mass and of the stellar mass on circular velo-

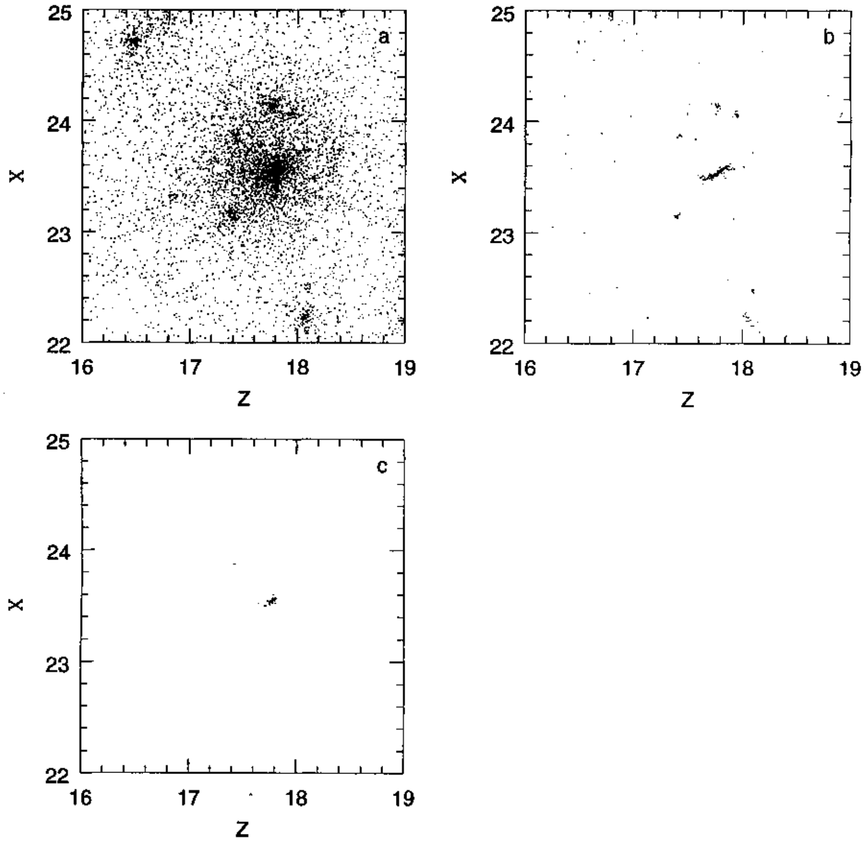

Figure 4. Projected distribution of (a) dark matter, (b) gas and (c) stellar mass for halo 3 at $z = 0$ in simulation 6 (1) and simulation 3 (2).

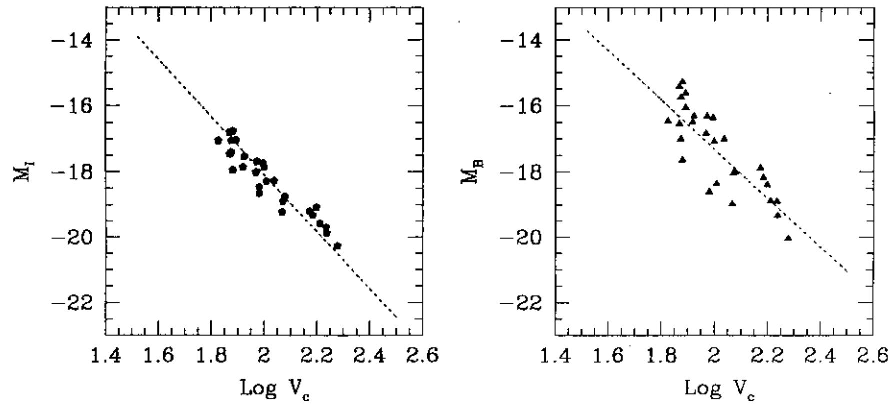

Figure 5. TF relation in the infrared (pentagons) and blue (triangles) bands for haloes in simulation 3. The corresponding observed TF (Pierce & Tully 1992) are shown for comparison (dashed line).

city. We considered two different subsamples according to the total baryonic particle number inside r_{200} in order to analyse the effects of the numerical resolution. According to Navarro & White (1993), the collapse of a gaseous clump (glob) can be reliably computed with a minimum of $N_{gas} \simeq 300$ particles. Consequently, we consider two subsamples of globs: subsample 1 with $N_{gas} \geq 300$, and subsample 2 with $N_{gas} \geq 30$. We computed the mass in stars (M_*) of the haloes as a function of circular velocity (V_c) for both subsamples. For subsample 1 we obtain $M_* \propto V_c^{2.8\pm0.3}$ and for subsample 2 $M_* \propto V_c^{3.3\pm0.2}$. According to White & Frenk (1991) the total virial mass and the circular velocity in galactic haloes satisfies $M_{vir} \propto V_c^3$. We find that the stellar content is also proportional to V_c^3, suggesting that SF does not strongly affect the accretion of baryonic mass into the potential well of the haloes. For the disc-like objects, we calculate their V_{rot} and M_b at 30 kpc (where V_{rot} is the rotational velocity of the disc and M_b is its baryonic content) finding $M_b \propto V_{rot}^{2.7}$. These results seem to disagree with Evrard, Summers & Davis (1994), where the authors found $M_b \propto V_{rot}^{1.7}$; however, after enforcing a rotational support correction, they got $M_b \propto V_{rot}^{2.5}$, a result that is consistent with ours.

We estimated the TF relation for the simulated galaxies in the blue and the infrared bands at $z=0$. As can be seen in Fig. 5, the slopes of the relations derived from the simulations are in reasonable agreement with the plotted observed values taking into account the observational error bands. Since, as already mentioned, the number of stars formed in the simulations is in excess compared with the observations, the zero-points of the simulated relations have been redefined to match the observations assuming a mass-to-light ratio $M/L = 9\ M_\odot/L_\odot$. It has to be stressed that objects with $V_c < 50$ km s^{-1} have not been included.

5 CONCLUSIONS

The aim of this paper is to present this new version of an AP3M hydrodynamical code. This code allows us to study the evolution of structure in a cosmological context including a correct treatment of pressure gradients, shocks and radiative cooling, as well as introducing a simplified treatment for SF. The code has been tested and results compared with others from existing codes. Although further improvement must be made in order to increase the dynamical resolution range of the code, the evolution of the structure and the study of their global astrophysical properties can be performed significantly well.

We also analysed the formation of structure in a typical region of a CDM universe, looking for hints to help us understand the physical processes involved and assess the performance of the code in this type of problem. From the analysis of the set of simulations performed, we may conclude the following:

(1) In agreement with previous works, we find that most of the gas settles into cold dense clumps that, in the absence of heating sources, remain at $T \propto 10^4$ K. The total cold gas mass in haloes exceeds the total stellar content observed in core galaxies, suggesting the need to introduce heating sources in order to reduce the overabundance of cold gas in clumps.

(2) Discs are formed through the accretion of substructure and, on average in our simulations, they settle at low redshifts ($z \simeq 0.5$). Mergers and accretion of objects of different sizes are very important in the evolution of galactic haloes given their high frequency (Tissera, Dominguez-Tenreiro & Goldschmidt 1996). It is observed in our simulations that, in general, discs can be regenerated after a merger.

(3) In models B we introduce a simple SF scheme as a first step towards building up a more realistic model of galaxy formation. The total amount of stellar mass found in galaxies in the simulations exceeds the observational value, resulting in a stellar density parameter that is 3–5 times greater than the observed one. When SF processes are included, the shape of the objects depends strongly on the efficiency parameter c chosen. For appropriate values we recover disc-like objects but at the price of shifting the SF to more advanced redshifts, in disagreement with observations. It has to be stressed that these simulations do not include feedback processes and that those mechanisms may have the ability to strongly affect the evolution of gas. Nevertheless, due to our poor understanding of these processes and actual numerical resolution limitations, it seems wise to first analyse the evolution of the structure without taking these factors into account and then to introduce feedback models as a second step.

(4) The baryonic mass accreted into the potential well of a halo is proportional to its total virialized mass, although slightly higher than $\Omega_b M_{vir}$. This result is not affected when SF is included and the relation $M_* \propto V_c^3$ remains valid.

(5) The inclusion of SF and stellar evolutionary tracks allows us to estimate the luminosities of the objects. The TF relation is marginally fitted in the infrared and blue bands depending on the observational constraints adopted. Supernovae may help us achieve a better fit at lower circular velocities, although it seems that they should not strongly affect objects with $V_c > 50$ km s^{-1}.

These results are the first outcome from the application of this version of AP3MSPH to the study of galaxy formation in a cosmological context. There are several points that require to be addressed more exhaustively. Future improvements of the code will permit us to increase the numerical resolution of the simulations enabling a better description of the joint evolution of the baryonic and dark matter.

ACKNOWLEDGMENTS

The authors thank Drs Efstathiou, White, Navarro, Frenk and Jones and the referee, Dr Steinmetz, for useful discussions and suggestions. We are grateful to the British Council, CONICOR, CONICET, the University of Cordoba, the University of Durham and the University of Cambridge for their support. PBT thanks Dr Efstathiou and the Astrophysics Department of the University of Oxford for providing a place and facilities to support her research.

REFERENCES

Benz W., 1990, in Buchler J. R., ed., The Numerical Modelling of Nonlinear Stellar Pulsations. Kluwer, Dordrecht, p. 180
Bertschinger E., 1985, ApJS, 58, 39
Cen R. Y., Jamenson A., Liu F., Ostriker J. P., 1990, ApJ, 326, L41
Charlot S., Bruzual G., 1991, ApJ, 367, 126
Cole S., Aragón-Salamanca A., Frenk C. S., Navarro J. F., Zepf S. E., 1994, MNRAS, 271, 781
Couchman H. M. P., 1991, ApJ, 368, L23
Couchman H. M. P., Thomas P. A., Pearce F. R., 1995, ApJ, 425, 797
Dalgarno A., McCray R. A., ARA&A, 10, 375
Davis M., Efstathiou G., Frenk C. S., White S. D. M., 1985, ApJ, 292, 371
Evrard A. E., 1988, MNRAS, 235, 911
Evrard A. E., Summers F. J., Davis M., 1994, ApJ, 422, 11
Frenk C. S., White S. D. M., Davis M., Efstathiou G., 1988, ApJ, 327, 507
Gingold R. A., Monaghan J. J., 1977, MNRAS, 181, 375
Hernquist L., Katz J., 1989, ApJS, 70, 419 (HK)
Katz N., 1992, ApJ, 391, 502
Kauffmann G., White S. D.M., Guiderdoni B., 1993, MNRAS, 264, 201
Lacey C. G., Guiderdoni B., Rocca-Volmerange B., Silk J., 1993, ApJ, 402, 15
Lucy L. B., 1977, AJ, 82, 1013
Miller F. E., Scalo J. M., 1979, ApJS, 41, 513
Monaghan J. J., 1992, ARA&A, 30, 543
Monaghan J. J., Gingold R. A., 1983, J. Comput. Phys., 52, 374
Monaghan J. J., Latanzio J. C., 1985, A&A, 149, 135
Mosconi M. B., Tissera P. B., Lambas D. G., 1994, in Franco J., Lizano S., Aguilar L., Daltabuit E., eds, Numerical Simulations in Astrophysics, Cambridge Univ. Press, Cambridge, p. 63
Navarro J. F., Benz W., 1991, ApJ, 380, 320
Navarro J. F., White S. D. M., 1993, MNRAS, 265, 271
Navarro J. F., White S. D. M., 1994, MNRAS, 267, 543
Navarro J. F., Frenk C., White S. D. M., 1995, MNRAS, 275, 56
Peebles P. J. E., 1980, The Large Scale Structure of the Universe. Princeton Univ. Press, Princeton
Peebles P. J. E., 1993, Principles of Physical Cosmology. Princeton Univ. Press, Princeton
Pierce F. R., Tully R. B., 1992, ApJ, 387, 47
Steinmetz M., Muller E., 1995, MNRAS, 276, 549
Summers F. J., 1994, PhD Thesis, Univ. of California of Berkeley
Thomas P. A., Couchman H. M. P., 1992, MNRAS, 257, 11
Tissera P. B., Abadi M., Lambas D. G., 1994, ApJ, 429, 29
Tissera P. B., 1995, PhD Thesis, Univ. of Cordoba, Argentina
Tissera P. B., Dominguez-Tenreiro R., Goldschmidt P., 1996, in Franco J., Terlevich R., Serrano A., eds, Proc. Rev. Mex. A.A. Conf. Ser., Vol. 6, Starburst Activity in Galaxies. p. 255
Umemura M., 1993, ApJ, 406, 361
White S. D. M., Frenk C., 1991, ApJ, 379, 52